

SCIENTIFIC REPORTS

OPEN

Penicimenolides A-F, Resorcylic Acid Lactones from *Penicillium* sp., isolated from the Rhizosphere Soil of *Panax notoginseng*

Received: 23 February 2016

Accepted: 18 May 2016

Published: 08 June 2016

Ya-Nan An^{1,*}, Xue Zhang^{1,*}, Tian-Yuan Zhang¹, Meng-Yue Zhang¹, Qian-Zhang², Xiao-Yu Deng¹, Feng Zhao², Ling-Juan Zhu¹, Guan Wang¹, Jie Zhang¹, Yi-Xuan Zhang¹, Bo Liu³ & Xin-Sheng Yao^{1,4}

Five new 12-membered resorcylic acid lactone derivatives, penicimenolides A-E (1–5), one new ring-opened resorcylic acid lactone derivative penicimenolide F (6), and six known biogenetically related derivatives (7–12) were isolated from the culture broth of a strain of *Penicillium* sp. (NO. SYP-F-7919), a fungus obtained from the rhizosphere soil of *Panax notoginseng* collected from the Yunnan province of China. Their structures were elucidated by extensive NMR analyses, a modified Mosher's method, chemical derivatization and single crystal X-ray diffraction analysis. Compounds 2–4 exhibited potent cytotoxicity against the U937 and MCF-7 tumour cell lines and showed moderate cytotoxic activity against the SH-SY5Y and SW480 tumour cell lines. The substitution of an acetyloxy or 2-hydroxypropionyloxy group at C-7 significantly increased the cytotoxic activity of the resorcylic acid lactone derivatives. Subsequently, the possible mechanism of compound 2 against MCF-7 cells was preliminarily investigated by *in silico* analysis and experimental validation, indicating compound 2 may act as a potential MEK/ERK inhibitor. Moreover, proteomics analysis was performed to explore compound 2-regulated concrete mechanism underlying MEK/ERK pathway, which is still need further study in the future. In addition, compounds 2–4 and 7 exhibited a significant inhibitory effect on NO production induced by LPS.

Panax notoginseng is widely distributed in Yunnan, Guangxi and Jiangxi province of China and its roots have been used as a traditional Chinese medicine for the treatment of hemorrhages, blood stasis and improvement of blood circulation and remission pain¹. In recent years, the investigations regarding the bioactive secondary metabolites from endophytic or rhizospheric fungi of *Panax notoginseng* have been receiving increasing attention, leading to the various secondary metabolites with antimicrobial^{2,3}, antifungal⁴, and cytotoxic activities⁵. During our studies for new natural bioactive constituents from rhizospheric fungus of *Panax notoginseng*, a strain of *Penicillium* sp. (SYP-F-7919) has drawn our interest because the EtOAc extract of the culture broth exhibited typical resorcylic acid lactones (RAL_s) UV absorptions (λ_{\max}) at 215, 264 and 297 nm⁶.

RALs are a class of fungal polyketide derivatives that are produced by a variety of fungal strains, such as *Lasiodiplodia theobromae*^{7,8}, *Penicillium* sp.⁹, *Syncephalastrum racemosum*¹⁰, *Pyrenophora teres*¹¹ and *Acremonium zeae*¹². Since the first RAL₁₂, lasiodiplodin, was isolated in 1971¹³, approximately 30 natural RAL₁₂ compounds had been obtained^{6–26}, some of which exhibit antibacterial^{15,16}, antifungal^{12,14}, antitumour^{10,17,18}, anti-inflammatory^{19,20,23}, antidiabetic²¹, and antihypertensive activities²². In our study, five new RAL₁₂ derivatives,

¹Shenyang Pharmaceutical University, Shenyang 110016, People's Republic of China. ²School of Pharmacy, Key Laboratory of Molecular Pharmacology and Drug Evaluation (Yantai University), Ministry of Education, Collaborative Innovation Center of Advanced Drug Delivery System and Biotech Drugs in Universities of Shandong, Yantai University, Yantai 264005, People's Republic of China. ³State Key Laboratory of Biotherapy and Cancer Center, West China Hospital, Sichuan University, and Collaborative Innovation Center of Biotherapy, Chengdu 610041, People's Republic of China. ⁴Institute of Traditional Chinese Medicine & Natural Products, College of Pharmacy, Jinan University, Guangzhou 510632, People's Republic of China. *These authors contributed equally to this work. Correspondence and requests for materials should be addressed to Y.-X.Z. (email: zhangyxzsh@163.com) or B. L. (email: liubo2400@scu.edu.cn) or X.-S.Y. (email: tyaoxs@jnu.edu.cn)

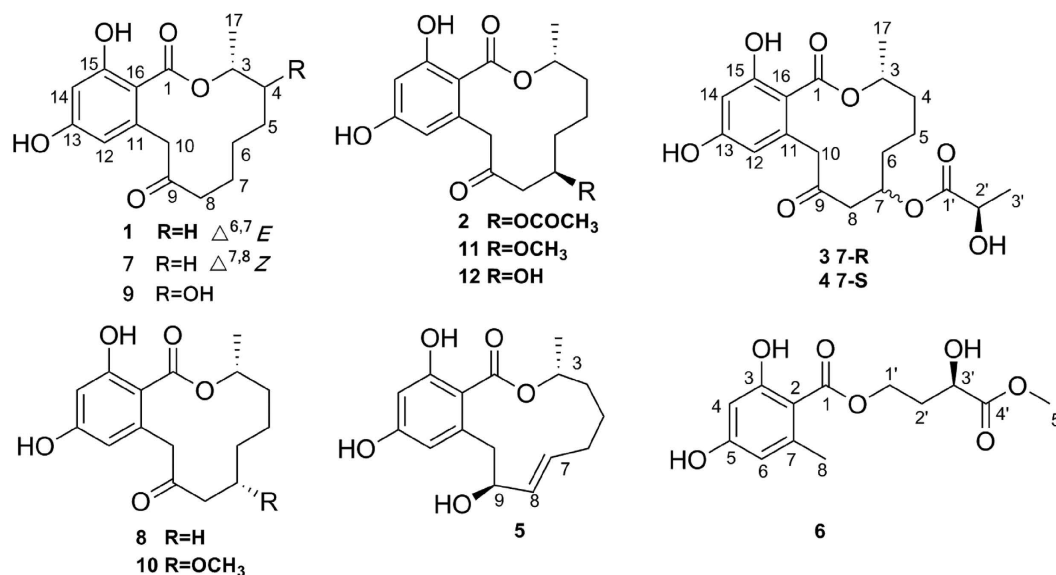


Figure 1. Chemical structures of compounds 1–12.

penicimenolides A–E (1–5), a new ring-opened resorcylic acid lactone derivative penicimenolide F (6), and six known biogenetically related derivatives (7–12) (Fig. 1) were isolated from the culture broth of the fungus. In the cytotoxicity assay, compounds 2–4 showed potent cytotoxic activity against the U937 and MCF-7 tumour cell lines and displayed moderate cytotoxicity against the SH-SY5Y and SW480 tumour cell lines. Subsequently, the possible mechanism of compound 2 against MCF-7 cells was preliminarily investigated by *in silico* analysis and experimental validation, indicating compound 2 may act as a potential MEK/ERK inhibitor. Moreover, proteomics analysis was performed to explore compound 2-regulated concrete mechanism underlying MEK/ERK pathway, which is still need further study in the future. In addition, compounds 2–4 and 7 exhibited a significant inhibitory effect on the production of nitric oxide (NO) in murine macrophages (RAW 264.7) activated by lipopolysaccharide (LPS). Herein, we report the isolation, structure elucidation, absolute configuration, bioactivities and preliminary mechanism of the compounds obtained from the *Penicillium* sp. SYP-F-7919.

Results and Discussion

Structural elucidation of resorcylic acid lactone derivatives. The ethyl acetate extract of the culture broth of the fungus *Penicillium* sp. was isolated by a combination of column chromatography, including silica gel, ODS, Sephadex LH-20, and reversed phase high performance liquid chromatography (HPLC) to yield twelve resorcylic acid lactone derivatives (1–12).

Penicimenolide A (1) was isolated as colourless needles, $[\alpha]_D^{25} + 68.1$ (*c* 0.5, MeOH). Its molecular formula was determined to be C₁₆H₁₈O₅ by HRESIMS at m/z 291.1231 [M + H]⁺ (calcd. for C₁₆H₁₉O₅, 291.1232). The IR spectrum of 1 revealed the presence of hydroxyl group(s) at 3384 cm⁻¹, carbonyl group(s) at 1708 and 1642 cm⁻¹ and an aromatic ring at 1605 and 1449 cm⁻¹. A comparison of the ¹H and ¹³C NMR spectroscopic data (Table 1) for 1 with those of 8 showed that the two compounds possessed a similar structure, except for the loss of two methylenes and the appearance of a pair of olefinic signals in 1. The coupling constant ($J_{6,7} = 15.5$ Hz) indicated an *E* configuration for the double bond. The position of the double bond was confirmed by the ¹H–¹H COSY correlations of H-6/H-5 and H-7/H-8 (Fig. 2). Because the absolute configuration at C-3 in 10 was identified to be *R* based on the X-ray diffraction analysis (Cu Ka) (Fig. 3), the asymmetric carbon atom C-3 in the isolated compounds (except for 6) was proposed to be an *R* configuration because of a shared biogenesis. For compound 1, this conclusion was further confirmed by comparing the optical rotation value with 8 ($[\alpha]_D^{25} + 40.7$). Based on the above evidence, the structure of 1 was identified to be (3*R*), (6*E*)-etheno-9-oxo-de-*O*-methylasiadiplodin.

Penicimenolide B (2) was obtained as colourless needles, $[\alpha]_D^{25} + 39.8$ (*c* 0.5, MeOH). The molecular formula C₁₈H₂₂O₇ was confirmed by HRESIMS at m/z 351.1435 [M + H]⁺ (calcd. for C₁₈H₂₃O₇, 351.1444). Except for an additional acetyl group, the ¹H and ¹³C NMR data (Table 1) for 2 were similar to those of 12. The HMBC correlation between H-7 and the carbonyl carbon of the acetyl group at δ_C 172.2 suggested that 7-OH was acetylated (Fig. 2). To confirm the absolute configuration of C-7 in 2, both compounds 2 and 12 were reacted with acetic anhydride and pyridine. Because of the same retention time in the HPLC analysis and the similar ¹H NMR data of the diacetylated derivative 2a and the triacetylated derivative 12a (see Supplementary Fig. S1), the absolute configuration of C-7 was confirmed to be *R*. Therefore, compound 2 was established to be (3*R*,7*R*)-7-acetoxy-9-oxo-de-*O*-methylasiadiplodin.

Penicimenolide C (3) was obtained as yellow needles, $[\alpha]_D^{25} + 15.4$ (*c* 0.5, MeOH) and was determined to have a molecular formula of C₁₉H₂₄O₈ on the basis of HRESIMS analysis (m/z 381.1549 [M + H]⁺, calcd. for C₁₉H₂₅O₈, 381.1549). The ¹H and ¹³C NMR data for 3 (Table 1) were similar to those of 2, except for an additional oxygenated methine (δ_H 4.21, δ_C 68.1). The HMBC correlations from H-7 (δ_H 5.51), H-2' (δ_H 4.21) and H₃-3' (δ_H 1.35) to C-1'

NO.	1		2		3	
	δ_C	δ_H	δ_C	δ_H	δ_C	δ_H
1	172.3 (C)		172.4 (C)		172.4 (C)	
3	74.8 (CH)	5.37 m	74.1 (CH)	5.16 m	74.1 (CH)	5.16 m
4	34.7 (CH ₂)	1.96 m;	34.0 (CH ₂)	1.65 m;	33.9 (CH ₂)	1.68 m;
		1.85 m		1.71 m		1.71 m
5	29.7 (CH ₂)	2.42 m;	19.2 (CH ₂)	1.56 m;	19.2 (CH ₂)	1.57 m;
		2.21 m		1.58 m		1.59 m
6	138.5 (CH)	5.60 dt (15.5, 6.9)	33.5 (CH ₂)	1.88 m;	33.4 (CH ₂)	1.89 m;
				1.56 m		1.61 m
7	122.5 (CH)	5.52 dt (15.5, 6.7)	71.6 (CH)	5.45 m	72.1 (CH)	5.51 m
8	46.2 (CH ₂)	2.99 m;	47.9 (CH ₂)	3.09 dd (15.9, 10.4);	47.7 (CH ₂)	3.14 dd (15.9, 10.4);
		2.99 m		2.68 dd (15.9, 1.4)		2.70 dd (15.9, 1.3)
9	208.2 (C)		206.7 (C)		206.6 (C)	
10	47.4 (CH ₂)	4.37 d (17.0);	52.9 (CH ₂)	4.55 d (18.7);	53.0 (CH ₂)	4.56 d (18.8);
		3.97 d (17.0)		3.85 d (18.7)		3.85 d (18.8)
11	139.1 (C)		139.9 (C)		139.9 (C)	
12	113.7 (CH)	6.12 d (2.5)	113.9 (CH)	6.11 d (2.5)	113.9 (CH)	6.11 d (2.4)
13	163.2 (C)		164.1 (C)		164.1 (C)	
14	103.1 (CH)	6.23 d (2.5)	103.2 (CH)	6.24 d (2.5)	103.2 (CH)	6.25 d (2.4)
15	165.5 (C)		167.0 (C)		167.0 (C)	
16	107.9 (C)		106.5 (C)		106.5 (C)	
17	19.3 (CH ₃)	1.34 d (6.5)	18.9 (CH ₃)	1.28 d (6.4)	18.9 (CH ₃)	1.29 d (6.4)
1'			172.2 (C)		175.1 (C)	
2'			21.3 (CH ₃)	2.01 s	68.1 (CH)	4.21 dd (13.8, 6.9)
3'					20.7 (CH ₃)	1.35 d (6.9)

Table 1. ¹H (600 MHz) and ¹³C NMR (150 MHz) data of 1–3 in CD₃OD (*J* in Hz).

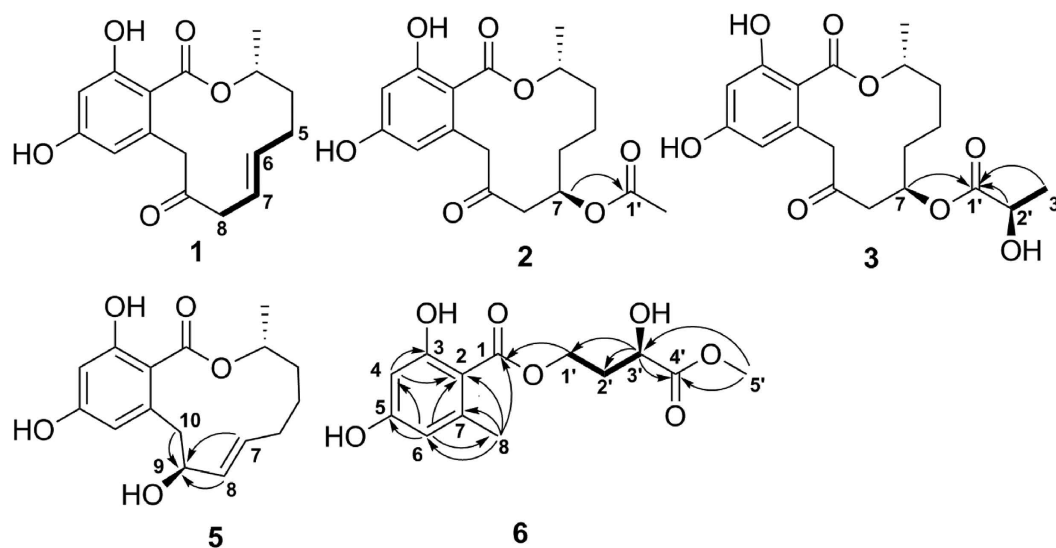


Figure 2. Key ¹H–¹H COSY (bold lines) and HMBC (arrows) correlations of 1–3, 5 and 6.

(δ_C 175.1), in combination with the ¹H–¹H COSY correlation between H₃–3' and H–2', revealed the presence of a 2'-hydroxypropionyloxy fragment attached to C-7 (Fig. 2). Accordingly, a planar structure was proposed for 3. The absolute configuration of C-2' in 3 was established using the modified Mosher method²⁷. Compound 3 was treated separately with (*R*)- and (*S*)-MTPA-Cl to obtain the respective (*S*)- and (*R*)-MTPA esters (3a and 3b). The *R* configuration of C-2' was determined by the positive $\Delta\delta_{H(S-R)}$ value of H₃–3' and the negative $\Delta\delta_{H(S-R)}$ value of H-7 (see Fig. 4 and Supplementary Table S2). In addition, the absolute configuration of C-7 was established by alkaline hydrolysis and HPLC analysis. Because of the same retention time of the alkaline hydrolysis product 3c ($[\alpha]_D^{25} - 58.2$) and the known compound 12 ($[\alpha]_D^{25} - 78.6$), the configuration of C-7 was confirmed to be *R*. Based

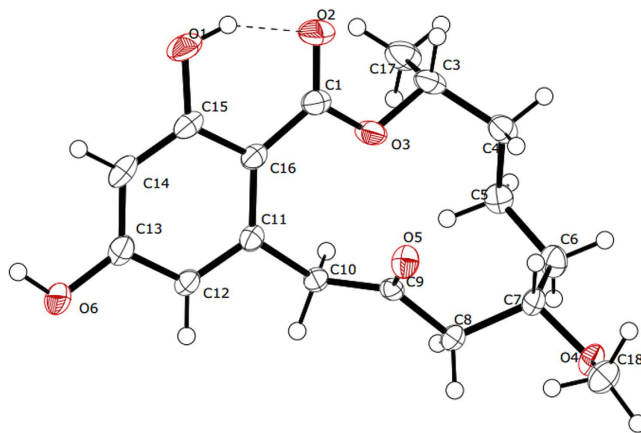


Figure 3. X-ray crystallographic structure of compound 10.

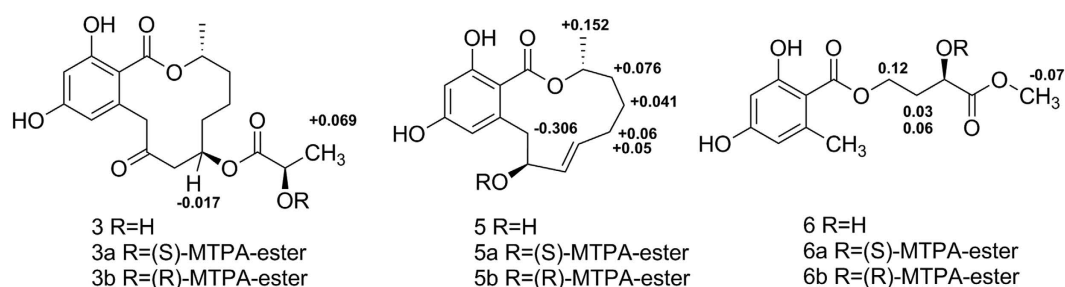


Figure 4. $\Delta\delta$ Values ($\delta_a - \delta_b$ in ppm) obtained for the MTPA esters of compounds 3, 5 and 6.

on the above evidence, the structure of **3** was determined to be (3*R*,7*R*,2'*R*)-7-(2'-hydroxypropionyloxy)-9-oxo-de-*O*-methylsiodiplodin.

Penicimenolide D (**4**) was isolated as a yellowish oil, $[\alpha]_D^{25} + 31.6$ (*c* 0.5, MeOH). The HRESIMS of **4** (*m/z* 381.1548 [$M + H$]⁺, calcd. for C₁₉H₂₅O₈, 381.1549) showed the same molecular formula as **3**. The ¹H and ¹³C NMR spectroscopic data for **4** (Table 2) were very similar to those for **3**. The analyses of the ¹H-¹H COSY, HSQC, and HMBC spectra of **4** indicated that the compound had an identical planar structure to that of **3**. A detailed comparison of the ¹³C NMR data for compounds **3** and **4** highlighted the differences in the chemical shifts at C-5, C-6, C-7 and C-8, suggesting that compound **4** is a C-7 epimer of **3**. Thus, the structure of **4** was determined to be (3*R*,7*S*,2'*R*)-7-(2'-hydroxypropionyloxy)-9-oxo-de-*O*-methylsiodiplodin.

To compare computed electronic circular dichroism (ECD) with experimental results is a valid method to assign absolute configurations of natural products^{28–32}. Thus, the absolute configurations of **3** and **4** were confirmed by quantum chemical TDDFT calculations of their ECD spectra. Conformational searches were performed using MMFF94S force field for **3** and **4**. All geometries (33 lowest energy conformers for **3** and 98 for **4**, respectively) with relative energy from 0–18 kcal/mol used in optimizations at the B3LYP/6-31G(d) level using Gaussian09 package³³. The B3LYP/6-31G(d)-optimized conformers (32 lowest energy conformers for **3**) with relative energy from 0 to 10 kcal/mol and conformers (28 lowest energy conformers for **4**) with relative energy from 0 to 10 kcal/mol were then re-optimized at the B3LYP/6-311+G(d) level. ECD computations for all conformers were carried out at the B3LYP/6-311++G(2d,p) level in the gas phase. Boltzmann statistics were performed for ECD simulations with standard deviation of σ 0.22 eV. The computed ECD of **3** and **4** were looked similar to the experimental values of **3** and **4**, respectively (Fig. 5). Thus, the absolute configurations of **3** and **4** were further confirmed.

Penicimenolide E (**5**) was obtained as a yellowish oil, $[\alpha]_D^{25} - 57.8$ (*c* 0.25, MeOH). Its molecular formula was confirmed to be C₁₆H₂₀O₅, which was deduced by the HRESIMS (*m/z* 293.1385 [$M + H$]⁺ calcd. for C₁₆H₂₁O₅, 293.1389). The detailed analysis of the ¹H and ¹³C NMR (Table 2) spectroscopic data revealed that **5** possessed a similar structure to *trans*-resorcylic⁶, and the only difference was the replacement of the ketone carbonyl at C-9 (δ_C 201.7) in *trans*-resorcylic by an oxygenated methine (δ_C 74.9) in **5**, which was further proven by the HMBC correlations from H-7, H-8, and H-10 to C-9 (Fig. 2). To confirm the absolute configuration of C-9 in **5**, a modified Mosher's method²⁷ was carried out to produce (S)- and (R)-MTPA esters (**5a** and **5b**). The negative $\Delta\delta_{H(S-R)}$ value of H-10 and the positive $\Delta\delta_{H(S-R)}$ value of H₃-17, H-4, H-5 and H-6 unambiguously confirmed the *S* configuration of C-9 (see Fig. 4 and Supplementary Table S3). Based on the above evidence, the structure of compound **5** was confirmed to be (3*R*,9*S*)-(7*E*)-etheno-9-hydroxy-de-*O*-methylsiodiplodin.

Penicimenolide F (**6**) was isolated as a yellowish oil, $[\alpha]_D^{25} - 4.6$ (*c* 0.25, MeOH). The HRESIMS exhibited a quasimolecular ion peak at *m/z* 285.0971 [$M + H$]⁺ (calcd. for C₁₃H₁₇O₇, 285.0974), indicating a molecular

NO.	4		5		6	
	δ_C	δ_H	δ_C	δ_H	δ_C	δ_H
1	172.6 (C)		170.8 (C)		173.0 (C)	
2					105.9 (C)	
3	76.1 (CH)	4.96 m	73.0 (CH)	5.08 m	166.4 (C)	
4	33.8 (CH ₂)	1.85 m;	33.4 (CH ₂)	1.93 m;	101.9 (CH)	6.15 d (2.4)
		1.76 m		1.66 m		
5	21.6 (CH ₂)	1.66 m;	22.5 (CH ₂)	1.70 m;	164.1 (C)	
		1.42 m		1.60 m		
6	34.0 (CH ₂)	1.74 m;	31.4 (CH ₂)	2.15 m;	112.7 (CH)	6.19 d (2.4)
		1.69 m		1.99 m		
7	70.8 (CH)	5.52 m	129.8 (CH)	5.49 dt (15.7, 6.3)	144.6 (C)	
8	50.1 (CH ₂)	2.99 dd (13.4, 3.0);	133.4 (CH)	5.35 dt (15.7, 5.2)	24.6 (CH ₃)	2.45 s
		2.63 dd (13.4, 10.3)				
9	207.3 (C)		74.9 (CH)	4.05 m		
10	51.0 (CH ₂)	4.77 d (18.5);	43.6 (CH ₂)	3.11 d (18.8);		
		3.77 d (18.5)		2.82 d (18.8)		
11	139.6 (C)		140.8 (C)			
12	114.1 (CH)	6.13 d (2.5)	111.1 (CH)	6.25 d (2.4)		
13	163.9 (C)		161.2 (C)			
14	103.1 (CH)	6.25 d (2.5)	102.3 (CH)	6.19 d (2.4)		
15	166.4 (C)		ND ^a			
16	106.9 (C)		115.1 (C)			
17	21.2 (CH ₃)	1.32 d (6.1)	19.0 (CH ₃)	1.31 d (6.4)		
1'	176.0 (C)				62.4 (CH ₂)	4.47 m
2'	68.1 (CH)	4.25 dd (13.8, 6.9)			34.4 (CH ₂)	2.24 m;
						2.06 m
3'	20.6 (CH ₃)	1.37 d (6.9)			68.9 (CH)	4.32 m
4'					176.1 (C)	
5'					52.7 (CH ₃)	3.68 s

Table 2. ¹H (600 MHz) and ¹³C NMR (150 MHz) data of 4–6 in CD₃OD (*J* in Hz). ^aDesignate signal not detected.

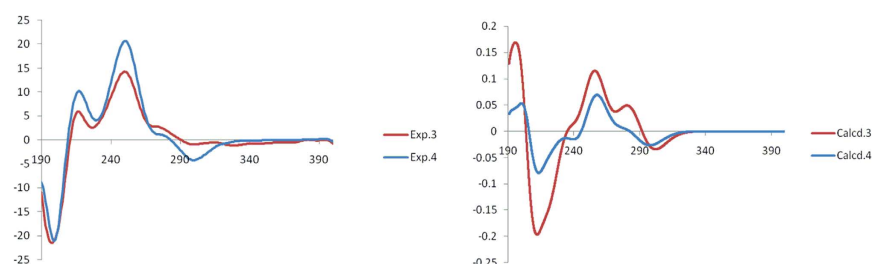


Figure 5. Calculated ECD spectra and experimental CD spectra of 3 and 4.

formula of C₁₃H₁₆O₇. The ¹H NMR spectrum of **6** (Table 2) showed two meta-coupled aromatic protons at δ_H 6.15 (d, *J* = 2.4 Hz, H-4) and 6.19 (d, *J* = 2.4 Hz, H-6), two methyl signals at δ_H 3.68 (s, H₃-5') and 2.45 (s, H₃-8), four methylene protons at δ_H 4.47 (m, H₂-1') and 2.06/2.24 (m, H-2'), and one methine proton at δ_H 4.32 (m, H-3'). The ¹³C NMR and DEPT spectra revealed the presence of 13 carbon resonances, including two ester carbonyls (δ_C 173.0, 176.1), six aromatic carbons, two methyls (one oxygenated), two methylenes (one oxygenated) and one oxygenated methine. The HMBC correlations (Fig. 2) from H-4 to C-1, C-2, C-3, C-5, and C-6, from H-6 to C-1, C-2, C-4, C-5, and C-8, and from H-8 to C-1, C-2, C-3, C-6, and C-7, combined with the molecular formula and the ¹³C NMR data, revealed the presence of a benzyloxy fragment with a methyl group located at C-7 and two hydroxyl groups at C-3 and C-5, respectively. The ¹H-¹H COSY correlations between H-1', H-3' and H-2', together with HMBC correlations from H₃-5' to C-3' and C-4' and from H-3' to C-1', C-2', and C-4', suggested the presence of a 3'-hydroxy-4'-oxo-4'-methoxy-butyl fragment, which was attached to the benzyloxy fragment, according to the correlation between H-1' and C-1 in the HMBC spectrum. Additionally, the absolute configuration of C-3' was established by a modified Mosher's method²⁷. The differences in the ¹H-NMR chemical shifts between (S)- and (R)-MTPA esters ($\Delta\delta_{H(S-R)}$) at H-1', H-2' and H₃-5' were analyzed to confirm the

Compound	IC ₅₀ (μM)					
	MCF-7	U937	SH-SY5Y	HepG2	SW480	A549
2	9.89 ± 0.41	1.38 ± 0.18	44.41 ± 1.42	>100	22.66 ± 1.22	>100
3	11.59 ± 0.23	6.49 ± 0.41	47.62 ± 0.81	>100	24.82 ± 1.85	>100
4	10.47 ± 0.44	2.19 ± 0.074	73.47 ± 1.62	>100	41.18 ± 2.3	>100
Taxol	0.0152	0.0553	0.454	1.562	1.845	1.512

Table 3. Cytotoxicity of compounds 2–4 against human tumour cell lines.

absolute configuration of C-3' as *R* (see Fig. 4 and Supplementary Table S4). Thus, the structure of compound 6 was determined to be (3'*R*)-3'-hydroxy-4'-oxo-4'-methoxy-orsellinate.

In addition, six known compounds were isolated and identified as *cis*-resorcylic acid (7)⁶, dihydroresorcylic acid (8)²⁴, (13*S*, 14*R*)-13-hydroxydihydroresorcylic acid (9)²⁵, (11*S*)-methoxyresorcylic acid (10)⁶, (11*R*)-methoxyresorcylic acid (11)⁶ and 7-hydroxydihydroresorcylic acid (12)⁶ by a comparison of the observed and published data.

Cytotoxicity of compounds against human tumour cell lines. Most of the isolated compounds (2–5, 7–12) were evaluated for their cytotoxic activity against six human tumour cell lines, including U937, MCF-7, A549, SH-SY5Y, HepG2 and SW480 (Table 3). Taxol, a well-known anticancer drug, was used as a positive control. Compounds 2–4 exhibited potent cytotoxicity against the U937 and MCF-7 cell lines, with IC₅₀ values ranging from 1.4 to 11.6 μM and showed moderate cytotoxic activity against the SH-SY5Y and SW480 tumour cell lines. In contrast, compounds 5 and 7–12 were inactive against the six tested cell lines. The above data indicated that the substitution of an acetyloxy or a 2-hydroxypropionyloxy group at C-7 significantly increased the cytotoxic activity of the resorcylic acid lactone derivatives.

Molecular docking of compound 2 with MEK1 and ERK1. Molecular docking is a widely used computational approach to screen potential active structures based on their interactions with the binding site³⁴. The predicted results obtained from SEA showed that our candidate compounds potentially chose MEK1 or ERK1 as a target. In this study, compound 2 was selected as a potential MEK1-ERK1 inhibitor, based upon its favorable “-CDOCKER ENERGY” scores. In order to understand the conformation of compound 2 in the ATP binding site of MEK1 and ERK1, molecular docking analysis and MD simulations were conducted to evaluate the binding affinity of compound 2 and MEK1, as well as ERK1.

After 3ns MD simulations, one frame (time of 3000ps) of the equalized trajectory was extracted, we found that compound 2 could bind to ATP binding domain of MEK1 and ERK1 stably. Compound 2 could form hydrogen bonds with residues Ala76, Asn78, Lys97, Gly210 and Val211 of the MEK1 (Fig. 6A). For ERK1, the hydrogen bonds were found between compound 2 and residue Lys71 and Asp123 of the ERK1, respectively (Fig. 6B). Moreover, we found compound 2 can form hydrophobic interactions in the hydrophobic pocket of MEK1 with lipophilic residue Val82. For ERK1 protein, the hydrophobic interactions were also formed with lipophilic residues Val56, Ala69, Met125 and Leu173. Altogether, these results suggest that compound 2 exhibits efficient binding to ATP binding domain of MEK1 and ERK1, which may support its inhibitory effect against MEK1 and ERK1.

Root mean square deviation (RMSD) fluctuation was an important criterion to gauge whether the protein-ligand system was stable. For MEK1-compound 2 system, RMSD of the complex were process about 2ns equilibrium during the whole simulation (Fig. 6C). During the process of MD simulation, RMSD of ERK1-compound 2 complex were limited to 0.3 nm, indicating a well-balanced system (Fig. 6D). Notably, we found RMSD of compound 2 in MEK1 protein remains stable after 800ps simulation, and then the RMSD fluctuations were narrow, indicating a stable binding in the ATP binding domain of MEK1 protein (Fig. 6C). The similar situation was also found in ERK1-compound 2 system, in which RMSD of compound 2 reached its dynamic equilibrium after 800ps simulation (Fig. 6D).

Compound 2 induces apoptosis through MEK/ERK pathway in MCF-7 cells. *In vitro* experiments were employed with MCF-7 cells to elucidate the possible mechanism of compound 2, as ERK are often excessively activated in breast cancer³⁵. Interestingly, we found that compound 2 demonstrated potent cytotoxic effect against MCF-7 cells in a time- and concentration-dependent manner, with an IC₅₀ value of 9.893 μM (24 h) (Fig. 7A). In order to determine features of cell death induced by compound 2, the morphologic changes of cells were examined by phase-contrast microscope. Compared with control group, compound 2 caused remarkable morphologic changes such as membrane blebbing and apoptotic bodies (Fig. 7B). These changes were further confirmed by Hoechst 33258 staining. The cells in control group showed uniform dispersion of low-density fluorescence, but compound 2 treated cells showed condensed, bright fluorescence and nuclear fragmentation (Fig. 7C). In addition, apoptotic ratio was further evaluated by Annexin-V/PI double staining. We found the early apoptotic cells ratio was increased from 1.68 ± 0.25% to 10.81 ± 2.47% (*p* < 0.05) and 27.53 ± 3.21% (*p* < 0.01), respectively, when treated with 10 μM and 15 μM of compound 2, indicating that compound 2 increases apoptotic ratio in a dose-dependent manner (Fig. 7D).

To further demonstrate compound 2 induced apoptosis, we investigated the involvements of apoptotic markers in compound 2-treated cells. We found that compound 2 significantly upregulated Bax expression as well as downregulated Bcl-2 expression. And the active form of PARP was also increased during compound 2 treatment (Fig. 7E). Based upon the molecular docking results of compound 2, we next examined the expression levels of MEK1/2 and ERK1/2. As expected, the phosphorylation of MEK1/2 and ERK1/2 were simultaneously decreased

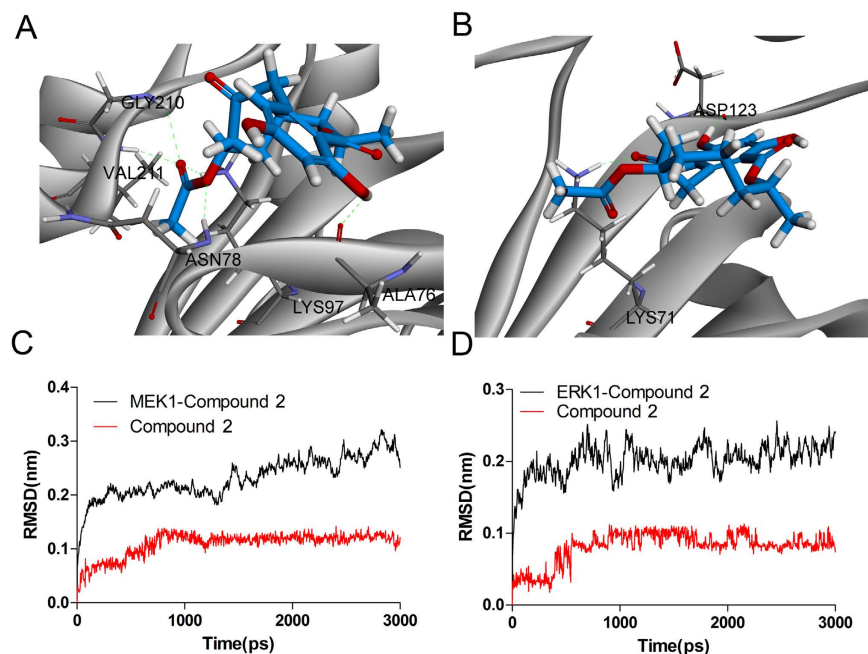


Figure 6. Binding analysis of compound 2 with the ATP binding domain of MEK1 and ERK1 proteins. (A) The binding model of compound 2 (colored red) with MEK1. Compound 2 and its hydrophobic surface in receptor residues were illustrated, from blue for hydrophilic to brown for hydrophobic, the important residues and their critical interactions (dash lines) with compound 2 in the binding site were depicted, conventional hydrogen bond, hydrophobic interactions were colored green and carnation, respectively. (B) The Binding model of compound 2 (colored marine) with ERK1. (C) RMSD of MEK1-compound 2 complex and compound 2 during the 3ns MD simulation. (D) RMSD of ERK1-compound 2 complex and compound 2 during the 3ns MD simulation.

after treatment of compound 2, as well as the decreased expression of total MEK1/2 and ERK1/2, which is in accordance with our previous prediction (Fig. 7F). These results demonstrate that compound 2 could induce apoptosis by targeting MEK1/2 and ERK1/2 in MCF-7 cells.

Proteomics-based analysis of potential apoptotic pathways. In order to study the potential molecular mechanisms of compound 2-induced apoptosis, we used iTRAQ and MS/MS analysis to profile differentially expressed proteins in compound 2-treated MCF-7. Based on high fold-change, we defined about thousands of differentially expressed proteins in compound 2-treated MCF-7 cells. A proteomics-based MEK1/ERK1-modulated PPI network that includes 67 differentially expressed proteins and 84 interactions was constructed (Fig. 8A). In view of the above results, in breast cancer MEK1/ERK1-independent pathways may play a role in the process of apoptosis. Subsequently, differentially expressed proteins in proteomics-based MEK1/ERK1-modulated PPI network was annotated in two colors (Fig. 8B) and the 139 apoptosis-related proteins were divided into 11 clusters in MCF-7 cells (Fig. 8C). These results may shed a light on the exploration of further mechanism study in the future.

Inhibitory effect of compounds on NO production. All of the isolated compounds, except for 1 and 6, were evaluated for their inhibitory effect on NO production in LPS-activated murine macrophages (RAW 264.7), as shown in Table 4. In this assay, hydrocortisone was used as a positive control. The cell viability was measured in parallel using the MTT method to exclude the bioactivity resulting from the cytotoxicity of the tested compounds. Compounds 2-4 and 7 showed a significant inhibitory effect on NO production, with the IC_{50} values ranging from 0.7 to 5.8 μ M. In addition, compounds 5, 8, 10 and 12 had weak activity.

The free radical NO, which is produced by the oxidation of L-arginine catalyzed by a group of nitric oxide synthases (NOSs), can be involved in a series of physiological and pathological processes³⁵. Many diseases, such as inflammation and cancer, have been reported to be associated with the overproduction of NO³⁶. Therefore, an inhibitor of NO production may be beneficial to the treatment of diseases induced by excessive concentrations of NO, especially in some malignant tumours. And of course, the great significance and possible mechanisms of these active compounds, as well as the relationship between their antitumour activities and NO inhibition activities remain to be further explored.

Methods

General Experimental Procedures. Melting points were determined with a Tektronix X-4 micromelting-point apparatus (Beijing, China). The optical rotations were recorded on a JASCO P-1020 digital polarimeter (Kyoto, Japan), and the UV spectra were measured with a Shimadzu UV-2201 UV-Vis recording

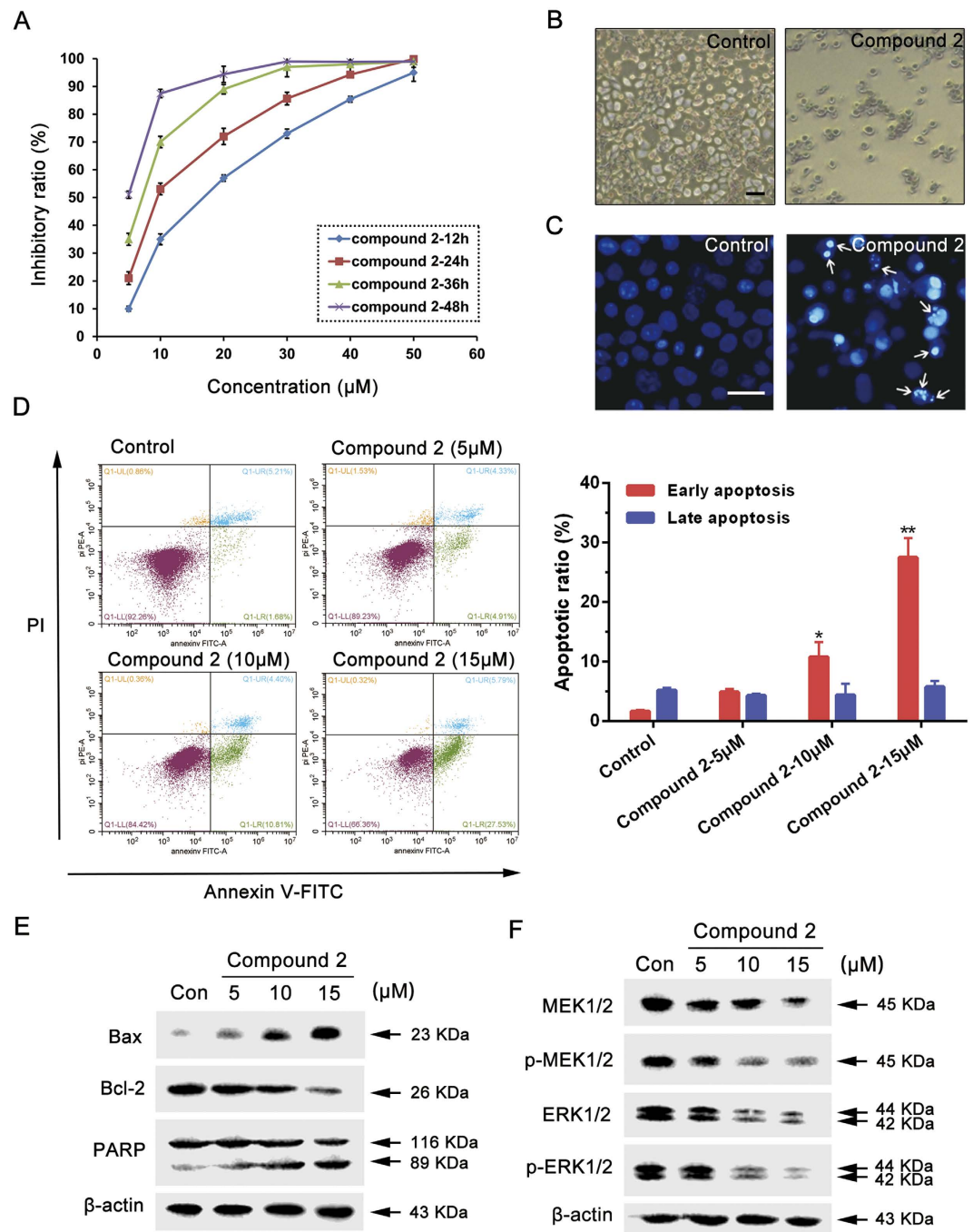


Figure 7. Compound 2 induces apoptosis in MCF-7 cells via targeting MEK/ERK pathway. (A) Effect of compound 2 on MCF-7 cell viability. The cells were cultured for 24 h, and then incubated with different concentrations of compound 2 for 12, 24, 36 and 48 h. The viability was determined by the MTT assay. The data are presented as the mean \pm SD of the results from three independent experiments. (B) The cells were treated with compound 2 (10 μ M) for 24 h, then observed by phase contrast microscope. Scale bar = 100 μ m. (C) The cells were treated with compound 2 (10 μ M) for 24 h then stained with Hoechst 33258 and observed by fluorescence microscope. Arrows indicate the apoptotic bodies. Scale bar = 50 μ m. (D) The cells were treated with different concentrations of compound 2 for 24 h, then revealed by Annexin-V/PI double staining using flow cytometry analysis. *Compared with control, $p < 0.05$, **Compared with control, $p < 0.01$. (E) The cells were incubated with different concentrations of compound 2 for 24 h, then the expression levels of Bax, Bcl-2 and PARP were detected by western blot analysis. Each lane was loaded with 30 μ g of whole cell extracts, β -actin was used as a loading control. (F) The cells were incubated with different concentrations of compound 2 for 24 h, then the expression levels of MEK1/2, p-MEK1/2, ERK1/2 and p-ERK1/2 were detected by western blot analysis. Each lane was loaded with 30 μ g of whole cell extracts, β -actin was used as a loading control.

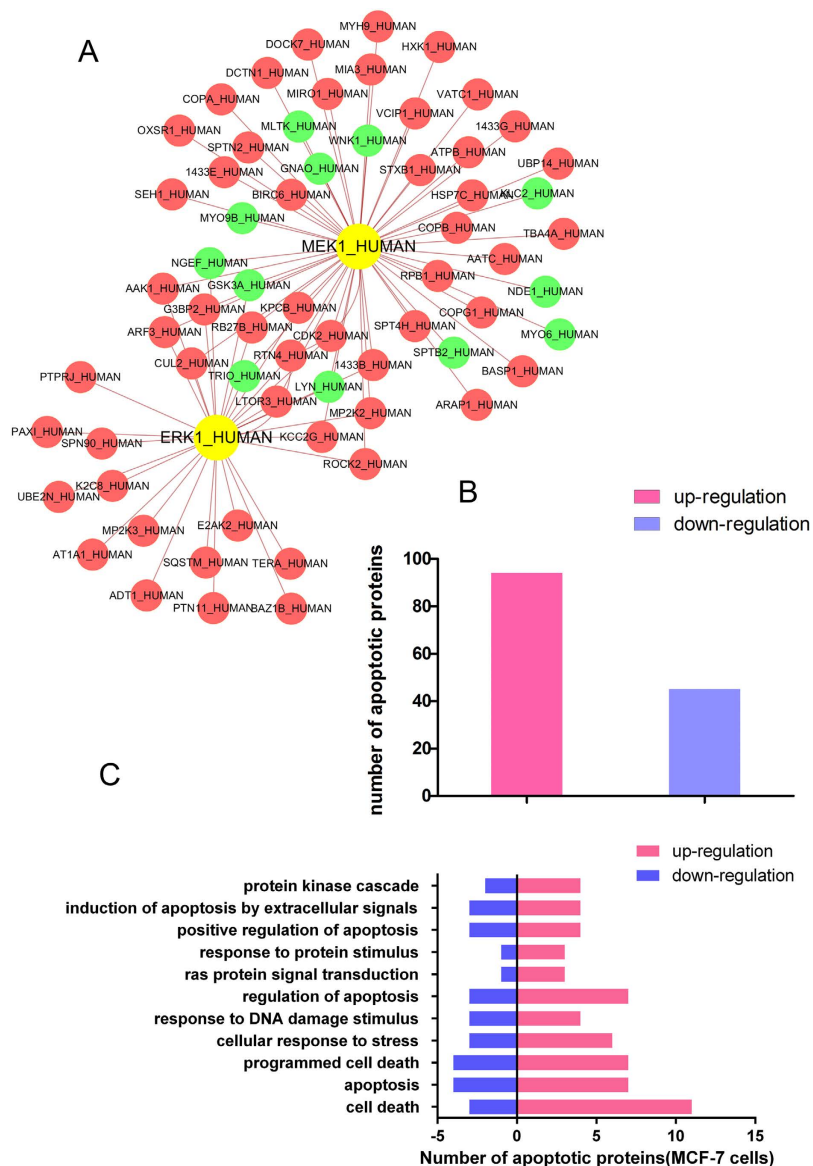


Figure 8. Proteomics analyses of compound 2-treated MCF-7 cells. (A) Proteomics-based identification of novel ERK1 or MEK1 apoptotic pathways in compound 2-treated MCF-7 cells. **(B)** The difference of protein levels (upregulation or downregulation) between control and compound 2-treated MCF-7 cells. **(C)** The apoptosis-related enrichment analyses of compound 2-treated MCF-7 cells.

Compound	IC ₅₀ (μM)
2	5.53 ± 0.39
3	5.79 ± 0.46
4	1.23 ± 0.10
5	68.39 ± 4.51
7	0.73 ± 0.06
8	73.93 ± 7.15
9	>100
10	70.45 ± 6.62
11	>100
12	55.94 ± 3.22
Hydrocortisone	48.66 ± 3.26

Table 4. Inhibitory effect of compounds 2–5 and 7–12 on NO production.

spectrophotometer (Kyoto, Japan). The IR data (KBr disks) were measured by a Bruker IFS-55 spectrometer (Rheinstetten, Germany). The CD spectra were obtained using a Bio-Logic MOS-450 (Grenoble, France). The 1D and 2D NMR spectra were run on Bruker AVANCE-400 or AVANCE-600 NMR spectrometers (Rheinstetten, Germany). The HRESIMS data were obtained on a Waters Synapt G2 QTOF mass spectrometer (MA, USA). The analytical HPLC was performed using an Agilent 1200 (CA, USA) equipped with a DAD detector using an ODS column (5 μ m, 250 \times 4.60 mm; Phenomenex Luna, CA, USA). Semipreparative HPLC was performed using a Shimadzu LC-6AD (Kyoto, Japan) equipped with a UV SPD-20A detector using an ODS column (5 μ m, 250 \times 10 mm, Phenomenex Luna, CA, USA). Column chromatography was carried out using silica gel (100–200 mesh and 200–300 mesh, Qingdao, China), ODS (60–80 μ m, Tokyo, Japan), and Sephadex LH-20 (Uppsala, Sweden). Analytical grade solvents were used for the extraction and chromatographic separation.

Fungal Material. The fungal strain used in this work was isolated from the rhizosphere soil of *Panax notoginseng*, which was collected from Wenshan, Yunnan province of China in November 2012. The fungus was identified on the basis of the DNA sequence of the internal transcribed spacer (ITS1-5.8S-ITS2 region). The sequence data derived from the fungal strain has been submitted and deposited in GeneBank with the accession number KU380346. BLAST search results revealed that the isolate belongs to the genus *Penicillium* and had a high sequence identity (99%) to the species *Penicillium menorum*. A voucher specimen (No. SYP-F-7919) was deposited at the School of Life Science and Biopharmaceutics, Shenyang Pharmaceutical University.

The fungal strain was cultured on plates of potato dextrose agar (PDA) at 28 °C for 5 days. The plates were washed with double distilled water (ddH₂O) to obtain conidial suspensions. To inoculate Erlenmeyer flasks (500 mL), 1 mL of conidial suspension was used, each containing 200 mL of the medium (which contained soluble starch 50 g, peanut powder 15 g, soybean flour 3 g, glucose 20 g, MgSO₄ 0.75 g, KH₂PO₄ 1.0 g and distilled water 1 L). Each flask was incubated at 28 °C on a rotary shaker at 150 rpm for 7 days. Large scale fermentation was carried out in 200 Erlenmeyer flasks (500 mL).

Extraction and Isolation. The fermentation broth (48 L) was centrifuged to separate the supernatant from the mycelia. The supernatant was extracted thoroughly with ethyl acetate (3 \times 48 L), and the organic solvent was concentrated under reduced pressure to afford the crude extract (18.6 g), which was subjected to column chromatography over silica gel and eluted with cyclohexane-EtOAc (10:0 to 0:10) and EtOAc-MeOH (10:0 to 0:10) to produce eleven fractions (A-K). Fraction F (2.0 g), which was eluted with cyclohexane-EtOAc (8:2, v/v), was subjected to an ODS column and a MeOH-H₂O stepwise gradient to obtain seven subfractions (F1-F7). Subfraction F5 (eluted with 60% MeOH, 325.4 mg) was further purified using a Sephadex LH-20 column that was eluted with CH₂Cl₂-MeOH (1:1). Then, it was purified by pHPLC using 55% MeOH to yield compounds **1** (4.5 mg, t_R 22.5 min), **7** (106.6 mg, t_R 25.3 min) and **8** (16.0 mg, t_R 36.2 min). Fraction G (eluted with cyclohexane-EtOAc, 7:3, 1.8 g) was applied to an ODS column that was eluted with a gradient of MeOH-H₂O to give seven subfractions (G1-G7). Subfraction G3 (eluted 40% MeOH, 45.9 mg) was purified by pHPLC (25% MeCN) to afford compounds **6** (7.6 mg, t_R 36 min) and **5** (15.5 mg, t_R 40 min). Compounds **2** (8.4 mg, t_R 45 min), **10** (140.0 mg, t_R 26.5 min) and **11** (85.0 mg, t_R 22.5 min) were obtained from subfraction G4 (60% MeOH eluate, 649.2 mg) by purification with pHPLC using 55% MeOH. Fraction H (3.0 g) was also obtained from the cyclohexane-EtOAc (7:3, v/v) eluate on silica gel CC and then was separated into ten subfractions (H1-H10) by ODC CC using MeOH-H₂O as the eluent. Subfractions H4 (40% MeOH eluate, 181.7 mg) and H5 (50% MeOH eluate, 106.0 mg) were purified by pHPLC (43% MeOH and 25% MeCN) to yield compounds **9** (10.5 mg, t_R 14.2 min) and **12** (15.5 mg, t_R 35 min), respectively. Compound **4** (10.0 mg, t_R 22.5 min) was purified from subfraction H6 (50% MeOH eluate, 162.6 mg) by pHPLC with 33% MeCN. Compound **3** (5.5 mg, t_R 40 min) was obtained from the subfraction H7 (60% MeOH eluate, 220.8 mg) using pHPLC (33% MeCN).

Acetylation of 2 and 12. A sample of compound **2** (5.0 mg) was dissolved in dry pyridine (1.0 mL), and Ac₂O (0.5 mL) was subsequently added. After stirring at 40 °C for 48 h, the mixture was concentrated in vacuo to dryness, and the residue was purified by pHPLC with MeCN-H₂O (35:65, v/v) at a flow rate of 4 mL/min to yield **2a** (1.0 mg). Following the above procedure, compound **12** was acetylated to yield **12a**.

Alkaline hydrolysis and HPLC analysis of 3. A mixture of compound **3** (5.0 mg) and 4% NaOH aqueous solution (5 mL) was stirred at 30–40 °C in a water bath for 3 h. The reaction mixture was neutralized with 10% HCl (4 mol/L) and extracted with EtOAc. After the extract was concentrated in vacuo to dryness, the residue was purified by pHPLC, eluting with MeCN-H₂O (25:75, v/v) at a flow rate of 4 mL/min to obtain the hydrolyzate **3c** (1.0 mg). Then, **3c** was compared to **12** by HPLC analysis, which showed that the retention time of the two compounds were identical (see Supplementary Fig. S2).

Penicimenolide A (1): colourless needles; mp 148–150 °C; [α]_D²⁵ +68.1 (c 0.5, MeOH); UV (MeOH) λ_{\max} (log ϵ) 215 (3.88), 265 (3.54), 302 (3.27) nm; CD (1.4 \times 10⁻³ M, MeOH) λ ($\Delta\epsilon$) 206 (-1.21), 217 (0.65), 290 (3.25), 330 (-0.05); IR (KBr) ν_{\max} 3384, 2920, 1708, 1642, 1605, 1449, 1384, 1262 cm⁻¹; ¹H NMR and ¹³C NMR data, see Table 1; HR-ESI-MS: *m/z* 291.1231 ([M + H]⁺, calcd. for C₁₆H₁₉O₅, 291.1232).

Penicimenolide B (2): colourless needles; mp 128–130 °C; [α]_D²⁵ +39.8 (c 0.5, MeOH); UV (MeOH) λ_{\max} (log ϵ) 214 (4.03), 262 (3.74), 302 (3.47) nm; CD (1.4 \times 10⁻³ M, MeOH) λ ($\Delta\epsilon$) 204 (-8.26), 224 (3.84), 260 (5.31), 306 (-1.01); IR (KBr) ν_{\max} 3405, 2921, 1722, 1646, 1619, 1449, 1384, 1362, 1263 cm⁻¹; ¹H NMR and ¹³C NMR data, see Table 1; HR-ESI-MS: *m/z* 351.1435 ([M + H]⁺, calcd. for C₁₈H₂₃O₇, 351.1444).

Penicimenolide C (3): yellow needles; mp 118–119 °C; $[\alpha]_{\text{D}}^{25} + 15.4$ (c 0.5, MeOH); UV (MeOH) λ_{max} (log ϵ) 213 (4.05), 262 (3.80), 301 (3.56) nm; CD (1.3×10^{-3} M, MeOH) λ_{max} ($\Delta\epsilon$) 208 (−8.05), 225 (1.51), 261 (5.34), 308 (−0.34); IR (KBr) ν_{max} 3426, 2920, 1727, 1644, 1452, 1384, 1261, 1207 cm^{-1} ; ^1H NMR and ^{13}C NMR data, see Table 1; HR-ESI-MS: m/z 381.1549 ($[\text{M} + \text{H}]^+$, calcd. for $\text{C}_{19}\text{H}_{25}\text{O}_8$, 381.1549).

Penicimenolide D (4): yellowish oil; $[\alpha]_{\text{D}}^{25} + 31.6$ (c 0.5, MeOH); UV (MeOH) λ_{max} (log ϵ) 220 (4.31), 264 (4.01), 303 (3.85) nm; CD (5.3×10^{-4} M, MeOH) λ_{max} ($\Delta\epsilon$) 209 (−2.91), 223 (0.74), 261 (4.81), 302 (−1.61); IR (KBr) ν_{max} 3417, 2920, 1752, 1645, 1606, 1458, 1384, 1261, 1189; ^1H NMR and ^{13}C NMR data, see Table 2; HR-ESI-MS: m/z 381.1548 ($[\text{M} + \text{H}]^+$, calcd. for $\text{C}_{19}\text{H}_{25}\text{O}_8$, 381.1549).

Penicimenolide E (5): yellowish oil; $[\alpha]_{\text{D}}^{25} - 57.8$ (c 0.25, MeOH); UV (MeOH) λ_{max} (log ϵ) 212 (3.94), 256 (3.27), 289 (3.07) nm; CD (6.8×10^{-4} M, MeOH) λ_{max} ($\Delta\epsilon$) 204 (4.65), 248 (−3.11), 285 (−0.70); IR (KBr) ν_{max} 3408, 2932, 1690, 1618, 1452, 1385, 1349, 1264 cm^{-1} ; ^1H NMR and ^{13}C NMR data, see Table 2; HR-ESI-MS: m/z 293.1385 ($[\text{M} + \text{H}]^+$, calcd. for $\text{C}_{16}\text{H}_{21}\text{O}_5$, 293.1389).

Penicimenolide F (6): yellowish oil; $[\alpha]_{\text{D}}^{25} - 4.6$ (c 0.25, MeOH); UV (MeOH) λ_{max} (log ϵ) 220 (4.16), 264 (3.97), 302 (3.59) nm; CD (7.0×10^{-4} M, MeOH) λ_{max} ($\Delta\epsilon$) 214 (5.49), 265 (−2.27), 298 (−2.18); IR (KBr) ν_{max} 3429, 2919, 1735, 1648, 1448, 1384, 1263 cm^{-1} ; ^1H NMR and ^{13}C NMR data, see Table 2; HR-ESI-MS: m/z 285.0971 ($[\text{M} + \text{H}]^+$, calcd. for $\text{C}_{13}\text{H}_{17}\text{O}_7$, 285.0974).

Crystallography data for compound 10. Colourless lump crystals of **10** were obtained from CHCl_3 containing a small amount of MeOH at room temperature. Crystallography data were obtained on an Agilent Super Nova (Dual, Cu at zero, Atlas) single crystal X-ray diffractometer with the Cu K α ($\lambda = 1.54184 \text{ \AA}$). Structure solution and refinement were performed with the SHELXL program package. The crystallography data for **10**: $\text{C}_{17}\text{H}_{22}\text{O}_6$; FW = 322.35; monoclinic space group P21, crystal size $0.40 \times 0.40 \times 0.30 \text{ mm}^3$, unit cell dimensions $a = 5.05804$ (7) \AA , $b = 11.74745$ (14) \AA , $c = 13.77837$ (18) \AA , $\alpha = \gamma = 90.00^\circ$, $\beta = 100.1922$ (13) $^\circ$, $V = 805.778$ (18) \AA^3 ; $Z = 2$; $T = 150 \text{ K}$; $D_{\text{calcd}} = 1.329 \text{ mg/m}^3$; $\mu = 0.836 \text{ mm}^{-1}$, $F(000) = 344$, 5093 measured reflections were collected, 3141 independent reflections [$R_{\text{int}} = 0.0167$]. Completeness to θ_{max} was 98.58%; Final R indices: $R_1 = 0.0140$ and wR_2 was 0.1007 [$I > 2\sigma(I)$]. The goodness of fit on F^2 was 0.971. Flack parameter = 0.08 (10).

The crystallography data for **10** were deposited in the Cambridge Crystallographic Data Centre (CCDC 1445050).

Cytotoxicity assay. The U937 and MCF-7 human cancer cell lines were obtained through commercial purchasing from American Type Cultures Collection (ATCC, Manassas, VA, USA). The A549, SH-SY5Y, HepG2 and SW480 human cancer cell lines were purchased from Life Science College Cell Resource Center of Chinese Academy of Sciences (Shanghai, China). The MCF-7, A549, SH-SY5Y and HepG2 cells were cultured in DMEM medium with supplement of 10% fetal bovine serum (FBS, Hyclone, USA). The U937 and SW480 cells were cultured in RPMI-1640 medium with supplement of 10% fetal bovine serum (FBS, Hyclone, USA). All these cells were cultivated in a 5% CO_2 humidified incubator at 37 °C. Cell lines in the phase of their growth cycle (6×10^4 cells/mL) were added to each well of 96-well plate (100 μL /well) and cultivated for 24 h. The tested compounds (**2–5**, **7–12**) were serially diluted in DMEM/RPMI-1640 at different concentrations and placed into wells in a total volume of 200 μL . Taxol (National Institutes for Food and Drug Control, China) was used as a positive control. After 24 h, 20 μL of MTT (3-(4,5-dimethylthiazol-2-yl)-2,5-diphenyltetrazolium bromide; 5 mg/ml) was added to each well. After a 4 h incubation, the supernatant was removed from the wells and the formazan crystals were dissolved in DMSO (150 μL). The plates were then shaken for 15 min, and the absorbance was measured at 570 nm using an enzyme immunoassay instrument (Thermo Scientific, USA).

Molecular docking. Target proteins of the small molecule compounds, were obtained from the similarity ensemble approach (SEA) (<http://sea.bkslab.org/>)³⁷. We downloaded the initial three-dimensional geometric coordinates of the X-ray crystal structure of MEK1 (PDB ID: 3W8Q) and ERK1 (PDB ID: 4QTB). Accelrys Discovery Studio version 3.5 (Accelrys Inc., USA) with CHARMM force field parameters were used to dock the pre-generated conformations of compound into MEK1 and ERK1, respectively. The CDOCKER to a rigid receptor with grid-based scoring was performed. By this way, the ligands were allowed to be flexible and structurally rearranged in response to the receptors. Finally, according to the “-CDOCKER INTERACTION ENERGY” and “-CDOCKER ENERGY” scores, the top ten ranked conformations for each ligand were finally preserved for further analysis.

Molecular dynamics (MD) simulations. To further verify the binding model of compound **2** with MEK1 and ERK1. MD simulations were carried out by GROMACS package (version 5.1.2)³⁸. Protein and small molecule compound were charged using amber99sb-ildn force field and general AMBER force field (gaff), respectively³⁹. The complex was solvated in a cubic box filled with TIP3P water molecules, the minimum distance from closest atom of solutes to edge of the box was define as 0.1 nm. Periodic boundary conditions (PBC) were used to avoid edge effects during the whole MD simulation. The charges of whole system were neutralized by adding an appropriate number Na^+ and Cl^- , so as to mimic a physiology concentration NaCl (0.15 M). Prior to operate the MD simulation, energy minimization was carried out to clear bad contacts. Then, 100ps NVT and 100ps NPT ensembles with simultaneous protein-ligand position restraints were also carried out to equilibrate the system. Consequently, 3ns MD production simulation was performed with a 2fs time step under constant temperature (300 K) and pressure (1 atm).

Hoechst 33258 staining. MCF-7 cells were seeded in each well of 6-well culture plates at a density of 2.5×10^5 cells/mL treated or untreated with compound 2 and cultured for 24 h. The subcellular structure alterations of apoptosis were observed under fluorescence inversion microscope.

Annexin-V/PI double staining. MCF-7 cells were seeded into 6-well culture plates with different concentrations of compound 2 and cultured for 24 h. The collected cells were then fixed with 500 μ L PBS. The apoptotic ratio was measured by flow cytometry (Becton Dickinson, Franklin Lakes, NJ) after employing Annexin-V-FLUOS Staining Kit (Roche, Germany).

Western blot analysis. MCF-7 cells were cultured in 6-well culture plates for 24 h. Then cells were treated with different concentrations of compound 2. All the cells were collected and were lysed by lysis buffer at 4 °C for 1 h. After 12,000 rpm centrifugation for 15 min, the protein level of the supernatant was quantified by Bio-Rad DC protein assay (Bio-Rad Laboratories, Hercules, CA, USA). Equal amounts of the total protein were separated by 12% SDS-PAGE and electrophoretically transferred to nitrocellulose membranes. Subsequently, membranes were blocked with 5% nonfat dried milk. Proteins were detected using primary antibodies (Danvers, MA, USA), followed by HRP-conjugated secondary antibody and visualized by employing ECL as the HRP substrate.

iTRAQ and MS/MS analysis. The iTRAQ and MS/MS analysis were performed in compound 2-treated MCF-7 cells. In simple terms, cells were dissolved in lysis buffer containing protease inhibitor (Sigma). Centrifuging the lysate for 1 h at 15 °C to get the supernatant, and stored it at -80 °C for further use. Protein quantitation was performed using Bio-Rad DC protein assay Kit (Bio-Rad). iTRAQ labeling was carried out using iTRAQ Reagent 4-Plex kit (AB SCIEX) based on the manufacturer's protocol with minor modifications. The whole cell lysates were labeled with iTRAQ labeling reagent 114 and 115 for the pair of control MCF-7 and compound 2-treated MCF-7, respectively. After 2D LC analysis and tandem mass spectrometry analysis, protein identification and relative iTRAQ quantification were performed with ProteinPilot™ Software 4.2 (AB SCIEX) using the Paragon™ algorithm for the peptide identification, which was further processed by Pro Group™ algorithm where isoform-specific quantification was adopted to trace the differences between expressions of various isoforms. Results with iTRAQ ratio cutoff values of 1.2 and 0.8 for fold-change and number cutoff values of 3 for quantifiable peptides for in protein abundance were accepted. Moreover, the results of 114 and 115 were adopted when their expression level were changed at the same trend.

Proteomics-based network construction of compound 2. To build the MEK1/ERK1 kinase protein-protein interaction (PPI) network, we collected diverse sets of biological evidence from seven online databases. Different PPIs were collected from the Database of Interacting Proteins (DIP)⁴⁰, Biomolecular Object Network Databank (BOND)⁴¹, Human Protein Reference Database (HPRD)⁴², HomoMINI⁴³, IntAct⁴⁴, BioGRID⁴⁵ and PrePPI⁴⁶. Moreover, we extracted the MEK1/ERK1 subnetwork from the PPI network based on the iTRAQ-based proteomics results.

Functional enrichment analyses. Differentially expressed proteins were assigned to 16 functional synaptic protein groups. Enrichment was only considered relevant when over represented functional groups contained at least 4 proteins. In addition, functional enrichment was determined using the DAVID functional annotation tool (<http://david.abcc.ncifcrf.gov/>). The functional categories used were GO term related to Biological Process (BP). And, the apoptosis-related proteins were detected and used as the background set.

NO production inhibition assay. Mouse monocyte-macrophages (RAW 264.7) were maintained in RPMI 1640 medium supplemented with penicillin (100 U/mL), streptomycin (100 μ g/mL) and heat-inactivated fetal bovine serum (10%) at 37 °C in a 5% CO₂ humidified incubator. The inhibition of NO production was evaluated by measuring the accumulation of nitrite (NO₂⁻) using a previously reported method^{47,48}. The RAW 264.7 cells were seeded in 96-well plates (200 μ L/well) at the initial density of 5×10^5 cells/mL in RPMI 1640 medium. After incubation for 1 h, the tested samples at various concentrations and LPS (Sigma, 1 μ g/mL) were simultaneously added to the wells. After being incubated at 37 °C for 24 h, the culture supernatant (100 μ L/well) was transferred to the enzyme-labelled plates and then mixed with an equal volume of Griess reagent. After 10 min at room temperature, the absorbance of the reaction products was measured at 540 nm. The cell culture without the tested compounds was used as the LPS group, the cell culture sample without the tested compounds and LPS was used as control group, and hydrocortisone was used as a positive control. All tests were performed in quadruplicate. The concentration of NO₂⁻ was calculated using a working curve of 1, 5, 10, 50 μ M NaNO₂ solutions, and the inhibitory rate on NO production was calculated by the level of NO₂⁻. Cytotoxicity was measured using a 3-(4,5-dimethylthiazol-2-yl)-2,5-diphenyltetrazolium bromide (MTT) colorimetric assay after 24 h of incubation with the tested compounds.

References

- Liu, L. *et al.* Protective effect of saponins from *Panax notoginseng* against doxorubicin-induced cardiotoxicity in mice. *Planta Med.* **74**, 203–209 (2008).
- Ding, G. *et al.* Sesquiterpenes and cyclopeptides from the endophytic fungus *Trioderma asperellum* Samuels, Lieckf. & Nirenberg. *Chem. Biodivers.* **9**, 1205–1212 (2012).
- Song, Y. P., Zhang, J. & Chen, G. Isolation and characterization of thiolutin from *Sterptomyces* sp. KIB0393. *Heteroletters* **5**, 21–26 (2015).
- Liu, K. *et al.* The antifungal metabolites obtained from the rhizospheric *Aspergillus* sp. YIM PH30001 against pathogenic fungi of *Panax notoginseng*. *Nat. Prod. Res.* **28**, 2334–2337 (2014).
- Yang, Y. B. *et al.* A new polyoxygenated farnesylcyclohexenone from Fungus *Penicillium* sp. *Nat. Prod. Res.* **30**, 65–68 (2016).

6. Barrow, C. J. New macrocyclic lactones from a *Penicillium* species. *J. Nat. Prod.* **60**, 1023–1025 (1997).
7. Yang, Q., Asai, M., Matsuura, H. & Yoshihara, T. Potato micro-tuber inducing hydroxylasiodiplodins from *Lasiodiplodia theobromae*. *Phytochemistry* **54**, 489–494 (2000).
8. Li, P., Takahashi, K., Matsuura, H. & Yoshihara, T. Novel potato micro-tuber-inducing compound, (3R,6S)-6-hydroxylasiodiplodin, from a strain of *Lasiodiplodia theobromae*. *Biosci. Biotechnol. Biochem.* **69**, 1610–1612 (2005).
9. Oyama, H., Sassa, T. & Ikeda, M. Structures of new plant growth inhibitors, *trans*- and *cis*-resorcylic. *Agric. Biol. Chem.* **42**, 2407–2409 (1978).
10. Buayairaksa, M. *et al.* Cytotoxic lasiodiplodin derivatives from the fungus *Syncephalastrum racemosum*. *Arch. Pharm. Res.* **34**, 2037–2041 (2011).
11. Nukina, M., Sassa, T., Oyama, H. & Ikeda, M. Structures and biological activities of fungal macrolides, pyrenolide and resorcylic. *Koen Yoshishu-Tennen Yuki Kagobutsu Toronkai* **22nd**, 362–369 (1979).
12. Poling, S. M., Wicklow, D. T., Rogers, K. D. & Gloer, J. B. *Acremonium zeae*, a protective endophyte of maize, produces dihydroresorcylic and 7-hydroxydihydroresorcylics. *J. Agric. Food Chem.* **56**, 3006–3009 (2008).
13. Aldridge, D. C., Galt, S., Giles, D. & Turner, W. B. Metabolites of *Lasiodiplodia theobromae*. *J. Chem. Soc.* **9**, 1623–1627 (1971).
14. Yang, R. Y. *et al.* Lactones from a brown alga endophytic fungus (No. ZZ36) from the South China Sea and their antimicrobial activities. *Bioorg. Med. Chem. Lett.* **16**, 4205–4208 (2006).
15. Xie, L. W. *et al.* Isolation and difference in anti-*Staphylococcus aureus* bioactivity of curvularin derivatives from the fungus *Eupenicillium sp.* *Appl. Biochem. Biotechnol.* **159**, 284–293 (2009).
16. Nair, M. S. R. & Carey, S. T. Metabolites of pyrenomyces XIII: Structure of (+) hypothemycin, an antibiotic macrolide from *Hypomyces trichothecoides*. *Tetrahedron Lett.* **21**, 2011–2012 (1980).
17. Lee, K. H. *et al.* Lasiodiplodin, a potent antileukemic macrolide from *Euphorbia splendens*. *Phytochemistry* **21**, 1119–1121 (1982).
18. Li, J. *et al.* Lasiodiplodins from mangrove endophytic fungus *Lasiodiplodia sp.* 318#. *Nat. Prod. Res.* **29**, 1–6 (2015).
19. Yao, X. S. *et al.* Biologically active constituents of *Arnebia euchroma*: Structure of arnebinol, an ansa-type monoterpenylbenzenoid with inhibitory activity on prostaglandin biosynthesis. *Chem. Pharm. Bull.* **39**, 2956–2961 (1991).
20. Fürstner, A. & Seidel, G. & Kindler, N. Macrocycles by ring-closing-metathesis, XI: syntheses of (R)-(+)-lasiodiplodin, zeranol and truncated salicylhalamides. *Tetrahedron* **55**, 8215–8230 (1999).
21. Yao, X. S. *et al.* Structure of arnebinol, a new ansa-type monoterpenylbenzenoid with inhibitory effect to prostaglandin biosynthesis. *Tetrahedron Lett.* **24**, 2407–2410 (1983).
22. Chen, S. H. *et al.* β -Resorcylic acid derivatives with α -glucosidase inhibitory activity from *Lasiodiplodia sp.* ZJ-HQ, an endophytic fungus in the medicinal plant *Acanthus ilicifolius*. *Phytochemistry Lett.* **13**, 141–146 (2015).
23. Jiang, C. S. *et al.* Synthesis, modification, and evaluation of (R)-de-O-methylasiodiplodin and analogs as nonsteroidal antagonists of mineralocorticoid receptor. *Bioorg. Med. Chem. Lett.* **21**, 1171–1175 (2011).
24. Xu, Y. *et al.* Insights into the biosynthesis of 12-membered resorcylic acid lactones from heterologous production in *Saccharomyces cerevisiae*. *ACS Chem. Biol.* **9**, 1119–1127 (2014).
25. Zhang, P. *et al.* Structure, absolute configuration, and conformational study of resorcylic acid derivatives and related congeners from the fungus *Penicillium brocae*. *RSC Adv.* **5**, 39870–39877 (2015).
26. Couladouros, E. A., Mihou, A. P. & Bouzas, E. A. First total synthesis of *trans*- and *cis*-resorcylic: remarkable hydrogen-bond-controlled, stereospecific ring-closing metathesis. *Org. Lett.* **6**, 977–980 (2004).
27. Su, B. N. *et al.* New chemical constituents of *Euphorbia quinquecostata* and absolute configuration assignment by a convenient Mosher ester procedure carried out in NMR tubes. *J. Nat. Prod.* **65**, 1278–1282 (2002).
28. Zhu, H. J., Li, W. X., Hu, D. B. & Wen, M. L. Discussion of absolute configuration for bioactive Griseusins by comparing computed optical rotations and electronic circular dichroism with the experimental results. *Tetrahedron* **70**, 8236–8243 (2014).
29. Yu, H. *et al.* Pestalotiopsis C, stereochemistry of a new caryophyllene from a fungus of *Trichoderma sp.* and its tautomerization characteristics in solution. *Tetrahedron* **71**, 3491–3494 (2015).
30. He, P. *et al.* Vibrational circular dichroism study for natural bioactive schizandrin and reassignment of its absolute configuration. *Tetrahedron Lett.* **55**, 2965–2968 (2014).
31. He, J. B. *et al.* Structure and absolute configuration of penicilliumine, a new alkaloid from *Penicillium commune* 366606. *Tetrahedron Lett.* **71**, 3491–3494 (2015).
32. Zhu, H. J. *Organic Stereochemistry—experimental and computational methods*, Wiley-VCH, Verlag GmbH & Co. KGaA, (2015).
33. Frisch, M. J. *et al.* Gaussian 09, revision A. 1, Gaussian, Inc., Wallingford CT, (2009).
34. Kitchen, D. B., Decornez, H., Furr, J. R. & Bajorath, J. Docking and scoring in virtual screening for drug discovery: methods and applications. *Biochim Biophys Acta.* **1773**, 1263–84 (2007).
35. Barnes, P. J. New anti-inflammatory targets for chronic obstructive pulmonary disease. *Nat. Rev. Drug Discov.* **12**, 543–559 (2013).
36. Coulter, J. A. *et al.* Nitric oxide—a novel therapeutic for cancer. *Nitric oxide* **19**, 192–198 (2008).
37. Keiser, M. J. *et al.* Relating protein pharmacology by ligand chemistry. *Nat. Biotechnol.* **25**, 197–206 (2007).
38. Abraham, M. J. *et al.* Gromacs: High performance molecular simulations through multi-level parallelism from laptops to supercomputers. *SoftwareX* **1–2**, 19–25 (2015).
39. Wang, J. *et al.* Development and testing of a general amber force field. *J. Comput. Chem.* **25**, 1157–1174 (2004).
40. Xenarios, I. *et al.* Dip: the database of interacting proteins. *Nucleic Acids Res.* **28**, 289–291 (2000).
41. Alfàrano, C. *et al.* The biomolecular interaction network database and related tools 2005 update. *Nucleic Acids Res.* **33**, D418–D424 (2005).
42. Mishra, G. R. *et al.* Human protein reference database-2006 update. *Nucleic Acids Res.* **34**, D411–D414 (2006).
43. Kerrien, S. *et al.* Intact-open source resource for molecular interaction data. *Nucleic Acids Res.* **35**, D561–D565 (2007).
44. Xu, Y. Z. *et al.* YL529, a novel, orally available multikinase inhibitor, potently inhibits angiogenesis and tumour growth in preclinical models. *Br. J. Pharmacol.* **169**, 1766–1780 (2013).
45. Winter, A. G., Wildenhain, J. & Tyers, M. Biogrid rest service, biogridplugin2 and biogrid webgraph: new tools for access to interaction data at biogrid. *Bioinformatics* **27**, 1043–1044 (2011).
46. Fu, L. L. *et al.* Systems biology network-based discovery of a small molecule activator BL-AD008 targeting ampk/zipk and inducing apoptosis in cervical cancer. *Oncotarget* **6**, 8071–8088 (2015).
47. Li, Y. X. *et al.* A new benzoquinone and a new benzofuran from the edible mushroom *Neolentinus lepideus* and their inhibitory activity in NO production inhibition assay. *Food Chem.* **141**, 1614–1618 (2013).
48. Jiao, W. H. *et al.* Dysifragilones A–C, unusual sesquiterpene aminoquinones and inhibitors of NO production from the South China Sea sponge *Dysidea fragilis*. *Eur. J. Org. Chem.* **2015**, 960–966 (2015).

Acknowledgements

The authors thank the Institute of Traditional Chinese Medicine and Natural Products, Jinan University for measuring the HRESIMS and optical rotation data. Thanks are also given to Prof. Hua-Jie Zhu and Dr. Fei Cao, at Hebei University for ECD calculation experiments. This work was supported by a grant from the Key Project of Yunnan Provincial Natural Science Foundation (2013FC008).

Author Contributions

X.-S.Y., Y.-X.Z., B.L. and X.Z. designed and coordinated the research. Y.-N.A. and J.Z. performed the isolation, purification and structure elucidation of the compounds. T.-Y.Z., M.-Y.Z., X.-Y.D. and Y.-X.Z. supplied the strain of *Penicillium* sp. (NO. SYP-F-7919) and finished the morphometric identification and fermentation. B.L. and Y.-N.A. carried out the cytotoxicity assay. F.Z. and Q.Z. conducted the NO production inhibition assay. B.L. and G.W. completed the investigation on the possible mechanism of compound **2** against MCF-7 cells. Y.-N.A., X.Z. and L.-J.Z. contributed to the manuscript writing. All authors reviewed the manuscript.

Additional Information

Supplementary information accompanies this paper at <http://www.nature.com/srep>

Competing financial interests: The authors declare no competing financial interests.

How to cite this article: An, Y.-N. *et al.* Penicimenolides A-F, Resorcylic Acid Lactones from *Penicillium* sp., isolated from the Rhizosphere Soil of *Panax notoginseng*. *Sci. Rep.* **6**, 27396; doi: 10.1038/srep27396 (2016).



This work is licensed under a Creative Commons Attribution 4.0 International License. The images or other third party material in this article are included in the article's Creative Commons license, unless indicated otherwise in the credit line; if the material is not included under the Creative Commons license, users will need to obtain permission from the license holder to reproduce the material. To view a copy of this license, visit <http://creativecommons.org/licenses/by/4.0/>